RESEARCH ARTICLE

VOLCANICA

The morphological response to the 13 May 2022 major explosive event at Stromboli volcano, Italy, characterised by high-resolution UAS surveys

Markus Schmid*[α], Ulrich Kueppers[α], Tullio Ricci[β], Riccardo Civico[β], Valeria Cigala[α], David Fee[γ, δ], Julia E. Gestrich[α, γ], Alexandra M. Iezzi[ε, ζ], Corrado Cimarelli[α], Caron E. J. Vossen[α], Richard M. Buzard[γ, η], Maurizio Ripepe[θ], Giorgio Lacanna[θ], and Donald B. Dingwell[α]

[α]Department of Earth and Environmental Sciences, Ludwig-Maximilians-Universität München, 80333 Munich, Germany.
[β]Istituto Nazionale di Geofisica e Vulcanologia, Sezione Roma 1, 00143 Roma, Italy.
[γ]Geophysical Institute, University of Alaska Fairbanks, Fairbanks, AK, USA.
[δ]School of Earth Sciences, Wills Memorial Building, University of Bristol, Bristol BS8 1RJ, UK.
[ε]U.S. Geological Survey, Volcano Science Center, Cascades Volcano Observatory, Vancouver, WA, USA.
[ζ]Department of Earth Science and Earth Research Institute, University of California, Santa Barbara, CA, USA.
[η]U.S. Geological Survey, Pacific Coastal and Marine Science Center, Santa Cruz, CA, USA.
[θ]Department of Earth Science, University of Florence, Firenze, Italy.

Submitted: 2024-05-22 | Accepted: 2025-07-19 | Published: 2025-08-26

Editor: J. Farquharson | Typesetter: J. Farquharson

Abstract

Since 2019, the frequency of major explosive eruptions at Stromboli volcano (Italy) has increased, heightening the exposure of population and scientists to the hazards posed by ejecta. Morphological changes can directly alter the hazard potential associated with these phenomena. Here, we present a quantitative morphological analysis of changes of the crater terrace area linked to the 13 May 2022 major explosive event. High resolution (2.5 cm pixel^{-1}) aerial imagery was acquired by unoccupied aircraft systems 2 hours before and 19 hours after the event. The 13 May 2022 major explosive event consisted of a minimum of seven explosions from four vents located in the south-central crater area. The opportune timing of this campaign enabled the quantification of morphological changes at Stromboli related to a single major explosive event at high temporal and spatial resolution. A total of 12.7×10^3 m^3 was excavated and 5.5×10^3 m^3 deposited. Via the mapping and classification of bomb distributions we observe that angular blocks make up the largest fraction of ballistics >0.2 m, from which we infer a strong interaction with wall rock and/or fragmentation of solidified plugs in the shallow plumbing system. The morphological changes observed provide valuable constraints on how much material is displaced, and the shift in location and the number of active vents during major explosive events at Stromboli.

Keywords: Stromboli; Explosive eruption; Eruption dynamics; UAS; Photogrammetry; Morphology.

1 Introduction

Stromboli volcano, Italy, is one of the world's most active volcanoes with recorded activity for the last 2000–2500 years [Rosi et al. 2000]. During recorded history, Stromboli's activity has been typically characterised by persistent, mild explosive activity interspersed infrequently by effusive episodes and less frequent but more energetic explosive events termed 'major explosions' and 'paroxysms' [Barberi 1993]. Major explosions can involve multiple vents emitting gas, pyroclastic jets to a few hundred metres above the vent, plumes that reach a few kilometres in height above mean sea level (AMSL), and the generation of small pyroclastic density currents. The duration of major explosions is usually between 30 and 40 s [Rosi et al. 2013]. The frequency of major explosions has been reported to be 1.7 events per year between 2002–2011 [Rosi et al. 2013], and 2.1 events per year in the period between 1895 and 1916 [Barberi 1993]. Between 28 August 2019 and 13 May 2022, 15 major explosions occurred, averaging to 5.5 events per year [Calvari and Nunnari 2023]. Paroxysmal activity has been reported to occur only once every few decades, typically characterised by powerful explosions lasting a few minutes that disperse ejecta out to a few kilometres from the vents. These events usually involve several active vents and may be accompanied by small-scale pyroclastic flows travelling out several hundreds of meters over the sea. As of late 2024, the most recent paroxysms occurred on 3 July and 28 August 2019 and on 11 July 2024. Textural and chemical analysis of the products of paroxysms at Stromboli revealed two recurrent types of pyroclasts (dark scoria and light pumices), suggesting the involvement of two distinct magma sources whereby volatile-rich magma coming from depths of ~7–10 km drives the paroxysms [e.g. Andronico et al. 2021; Giordano and De Astis 2021; Visalli et al. 2023]. Statistically robust textural analysis of ballistics of major explosions is more difficult as fewer ballistics reach areas accessible for sampling. Detailed information about such recent paroxysms at Stromboli can be found, for example, in Ripepe et al. [2008], Bertagnini et al. [2011], Calvari et al. [2012], Bevilacqua et al. [2020], Giudicepietro et al. [2020], Giordano and De Astis [2021], Calvari and Nunnari [2023], and Civico et al. [2024]. Following the paroxysms in 2019, the frequency of major explosions increased to several events per year [Calvari and Nunnari 2023], resulting in the closure of the summit area to tourism. In their *a posteriori* analysis of geophysical monitoring signals, Ripepe et al.

*markus.schmid@min.uni-muenchen.de

[2021] suggested that a timely automatic warning system for the detection of strain precursors may precede the occurrence of a paroxysmal event by about 10 minutes. Despite these promising results, lower magnitude major explosions remain challenging to forecast, posing a threat to people near active areas. In order to reduce this threat, the different processes that are involved in the various types of eruptive activity at Stromboli need to be better understood.

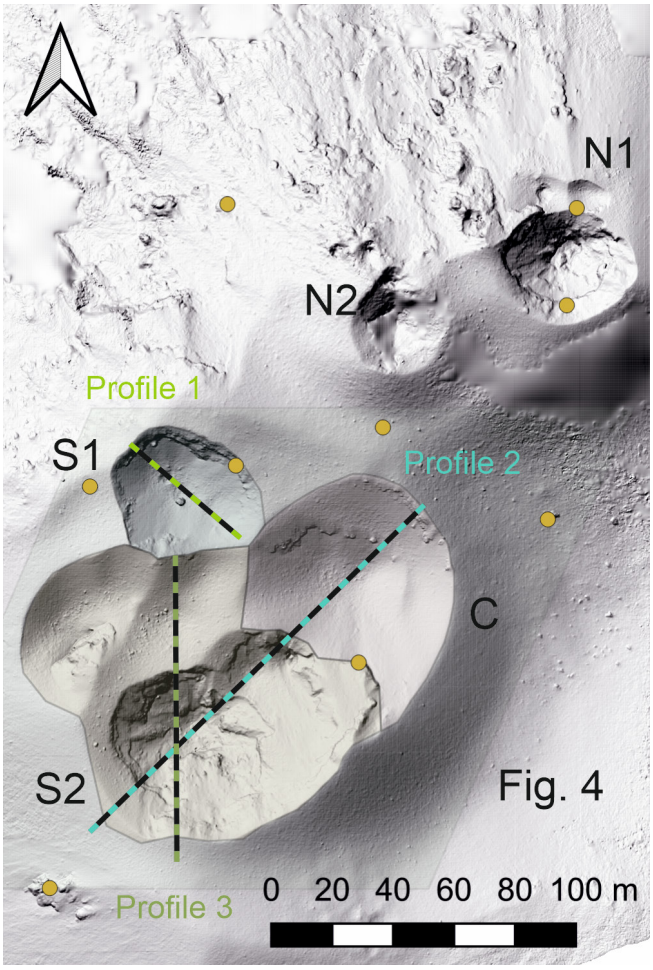

Figure 1: Shaded relief image of a DEM of Stromboli's crater terrace as visible on 13 May 2022 before a major explosive event, showing two distinct crater areas. The north-east crater area (N) consisted of two main vents, N1 and N2, and several smaller vents north of N1 and N2. The south-central crater area consisted of S1, S2, and the C vents, with S2 being subdivided into two distinct vents. Coloured lines mark the location of the sections through S1 and S2 craters shown in Figure 6 and Supplementary Material 1 Figure S2. Yellow points mark the location of the control points used for DEM alignment.

The use of unoccupied aircraft systems (UAS) in volcanic environments has increased steadily in recent years as a tool for mapping volcanoes [e.g. Turner et al. 2017; Darmawan et al. 2018; De Beni et al. 2019; Zorn et al. 2020; Civico et al. 2021; Dietterich et al. 2021; Schmid et al. 2021], sampling [e.g. Liu et al. 2019; Nadeau et al. 2020; Galle et al. 2021; MacLeod et al. 2023], and the deployment of instruments [Iezzi et al. 2023; Schmid et al. 2023]. For an overview of UAS volcanological applications we refer the reader to James et al. [2020a] and Lev [2022] and references therein.

Active volcanoes are highly dynamic in their geomorphology and changes of their topography are, for the most part, a direct representation of the eruptive activity. By resolving these changes through time, we can gain insight into the processes shaping the volcano. In this context it is important to tie together various observations of, for example, eruption volumes, pressure, and the related geophysical signals to allow a fine tuning of the interpretation of the forces at play and potential precursory signals. However, achieving the required spatial or temporal resolution to investigate changes from individual events can be challenging at volcanoes with frequent activity like Stromboli, as changes during normal Strombolian activity are too small to be resolved and/or, in case of larger events, it is difficult to get the timing right to obtain a dataset just before and after an event.

In May 2022, we conducted a multiparametric field campaign at Stromboli volcano involving several UAS platforms for photogrammetry and sensor deployment, acoustic and infrasound networks, and lightning detectors as well as high-speed optical and thermal cameras. During this campaign, a major explosion occurred on 13 May 2022 at 14:43 UTC that was recorded with several instruments, including opportune UAS photogrammetry surveys 2 hours before and 19 hours after the explosive event. These surveys provide unprecedented temporal resolution to analyse morphological changes to the summit crater geometry at Stromboli induced by a single major explosive event. As the post-eruption UAS data acquisition took place the following day in the morning, we assume that normal Strombolian activity did not alter the evaluated morphological changes significantly. Here we describe the acquisition and processing of aerial imagery and quantify the changes due to the major explosion.

2 Geological background

Stromboli volcano has been the subject of scientific interest for decades, resulting in an impressive volume of literature dedicated to unlocking the mechanisms driving its volcanic activity at depth and its surficial expression. Here, we focus our attention on the topography of Stromboli's crater terrace where all active vents are located (Figure 1). At the time of the survey, the crater terrace was at an elevation of ~810–860 m AMSL and hosted several active and inactive vents and craters. The crater terrace is subdivided into the north-east crater area (N) and the central-south crater area (CS) (Figure 1). In the N area, two vents (N1 and N2) were active during the campaign (9–14 May 2022) (Supplementary Material 1 Figure S1). In the optical UAS images, six smaller vents were visible in the N area. These vents generated no explosive activity during the time of observation although some showed active degassing or visible incandescence. The CS area consisted of around five nested crater structures with four visible vents, of which only the S2 vent exhibited activity. A notable feature of crater S1 is a solidified lava plug protruding from the surrounding excavated debris inside the crater (Figure 2). The activity in the days prior to the major explosion (during our visual observations)

was characterised by Strombolian explosions from N1, varying in intensity between gas jetting and ash-rich plumes that buoyantly rose to a few hundred meters above the vents and bombs that fell in close proximity of the craters [Gestrich et al. 2023]. In contrast, S2 exhibited explosions of lower intensity, manifested by <100 m ash and gas plumes. As a result of the 13 May 2022 major explosion, the location of S1 changed, with the new vent exhibiting a highly asymmetric geometry.

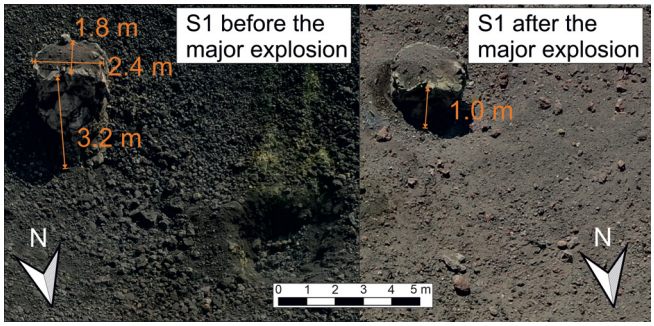

Figure 2: Solidified plug in vent S1 as visible on 10 and 14 May 2022. The diameter of the plug was measured from the UAS derived three-dimensional reconstruction. The visible vent before the explosion is located on the north-western side of the plug. The new vent, that was active during the 13 May 2022 major explosive event, formed south-east of the plug and moved the plug around two meters toward the NW.

3 Methods

Structure-from-motion photogrammetry was performed on aerial images obtained by UAS flights to quantify topographic changes. We used a DJI Phantom 4 real-time kinematic (RTK) UAS for the survey on 13 May 2022 at around 11:40 UTC in combination with the DJI D-RTK2 Mobile Station for RTK corrections through Network Transport of RTCM via Internet Protocol (NTRIP). For the post-eruption survey on 14 May 2022 at around 10:10 UTC we used a DJI Mavic 2 Pro. We followed best-practice suggestions (e.g. RTK, off-nadir camera angle, and reporting of processing parameters) by Eltner et al. [2016] and James et al. [2019, 2020b] to mitigate systematic errors. Both flights were conducted manually as grid-like and/or circular flight paths (Supplementary Material 1 Figure S2) around the vents with complex geometries with off-nadir camera angles at flight heights around 100 m above the crater terrace. This results in an approximate ground sample distance (GSD) of 2.4 cm pixel^{-1} for 13 May and 2.5 cm pixel^{-1} for 14 May 2022. The cameras were set to shutter priority mode with high shutter speeds (1/320–1/400) to ensure sharp images even from a moving UAS.

The Phantom 4 RTK has a camera with a 20 MP 1" CMOS sensor, an 8.8 mm/24 mm (35 mm equivalent) focal length, mechanical shutter, and a resolution of 5472 × 3648 pixels. The camera of the Mavic 2 Pro has similar specifications but has a 10.2 mm/28 mm (35 mm equivalent) focal length and an electronic shutter.

`Agisoft Metashape Professional` (Version 2.1.0) was used for the photogrammetric processing of the images. The images were first imported into the software, including the camera location accuracy from the image metadata. Images showing mostly gas or ash plumes were discarded. Smaller areas of degassing or ash plumes as well as background were manually masked to exclude these pixels during image alignment (128 and 220 images for 13 and 14 May 2022, respectively). During image alignment a sparse point cloud was created that was subsequently filtered to remove points with poor camera geometry during triangulation of points, large pixel matching errors, and large pixel residual errors. In between each filter run `Metashape`'s optimisation was used to reduce reprojection errors, resulting in lower root mean squared error (RMSE). Further information on processing parameters of `Agisoft Metashape Professional` and general workflows can be found in Over et al. [2021]. From the resulting sparse cloud, the dense cloud is generated and manually cleaned to remove floating points caused by the presence or insufficient masking of volcanic gas plumes. Floating points are easily recognized as they are detached from the surface and usually have a brighter colour since they are artefacts from reconstructing gas and vapor plumes.

The images taken by the Mavic 2 Pro were processed identically but without the information on the camera location accuracy which is only available in the dataset of the RTK-enabled UAS. The alignment of both dense clouds was realised in `Agisoft Metashape` by selecting nine visually identifiable reference points at geological features that remained unchanged during the major explosion (Figure 1). Since the dataset of 13 May 2022 is georeferenced by the RTK-corrected global navigation satellite system (GNSS) information embedded in the image data, we aligned the 14 May 2022 dataset to the previous dataset, treating the locations of the 9 reference points as ground control points (GCPs) to align both datasets in the 3D space. Additionally, the same nine reference points were used during the "align chunks" feature of `Agisoft Metashape`, in order to minimise the reprojection error (difference between observed image points and the predicted positions of these points in the 3D model) by adjusting camera position and orientations as well as 3D point positions (linear shifts and rotations) of the non-RTK dataset. The overall reprojection error is report as RMSE of 31.3 cm (X error 22.6 cm, Y error 18.0 cm, Z error 12.1 cm).

After the alignment, digital elevation models (DEMs) and orthomosaics were generated and exported to be analysed with `QGIS` (Version 3.34.2). The DEMs have a resolution of 4.95 cm pixel^{-1} and 4.63 cm pixel^{-1} for 13 and 14 May 2022, respectively. In order to allow accurate volume calculations, the DEMs have been resampled to matching cell sizes (5.0 cm pixel^{-1}). The resolution for the orthomosaics is 2.48 cm pixel^{-1} (13 May 2022) and 2.31 cm pixel^{-1} (14 May 2022). With `QGIS` the DEM of 14 May was georeferenced to the 13 May reference to further decrease the XY alignment error (from 5.78 pixel to 2.3 pixel, i.e.11.5 cm) by applying the best transformation to match the reference points (Figure 1) from both datasets, using a Helmert transformation. The parameters for the processing of the datasets in `Agisoft Metashape` were set to high, for image alignment accuracy and point cloud build quality with aggressive depth filtering. The

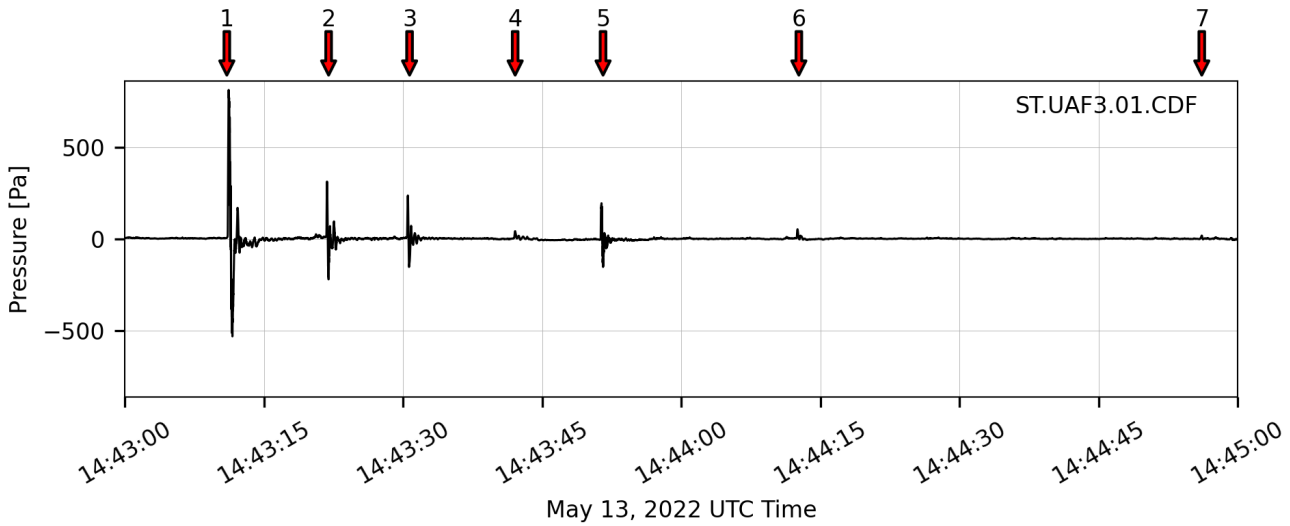

Figure 3: Infrasound waveforms for the 13 May 2022 major explosive event. Data are unfiltered and from station UAF3, deployed ~550 m from the S crater. At least seven distinct explosions are detected and marked by red arrows at the top of the plot.

use of the setting "high" ensures that the full resolution of the aerial images is used, while aggressive filtering removes outlying points that are not connected to the surrounding surface. See Table 1 for details about the photogrammetric survey and datasets and Supplementary Material 1 Table S1 for processing parameters.

The DEMs were used to calculate the elevation and volumetric changes caused by the major explosion on 13 May 2022 while orthomosaics were used to map bomb dispersal on the crater terrace. Bisson et al. [2023] and Bevilacqua et al. [2024] demonstrated the feasibility of using high-resolution orthomosaics to analyse ballistic distribution of the 3 July 2019 paroxysm at Stromboli. While these two studies focus on the size distribution of spatter bombs in areas that are also accessible by foot, we utilise high-resolution orthomosaics to evaluate bomb distribution and bomb characterisation in areas that cannot be accessed safely. The resolution of $<2.5\ \mathrm{cm\,pixel^{-1}}$ allowed a confident visual classification for pyroclasts larger than around 0.2 m. The classification was done by switching between the pre- and post-explosion orthomosaic to identify bombs that were already present. By comparing post-explosion orthomosaic and aerial images bombs were classified visually and outlines were manually drawn around the bombs in QGIS (Supplementary Material 1 Figure S3). Identification and classification of the more numerous clasts smaller than 0.2 m was not possible with high enough certainty to be included in the analysis. The distinction between bomb types (blocks/spatter) was done visually and manually based on bomb shape, surface morphology and colour. From the outlines around the clasts, their areas were measured and their equivalent diameter calculated. To estimate the volume of bombs >0.2 m we used the equivalent diameter as equivalent spherical diameter for blocks and we assumed a thickness of 0.2 m for spatter bombs that we multiplied by their measured area.

The 13 May 2022 major explosive event was clearly recorded on permanent and this campaign's temporary infrasound stations deployed around Stromboli's summit crater. See Iezzi et al. [2023] for more details on the campaign infrasound network. These stations provide information on the timing, number, location, and energetics of the explosions. The campaign infrasound stations consisted of Chaparral 60 UHP and Vx2 infrasound sensors connected to DATA-CUBE digitizers sampling at 400 Hz. They recorded at least seven distinct explosions in a period of two minutes during the major explosive event (Figure 3). The first explosion had the highest amplitude at over 800 Pa at station UAF3 at ~550 m distance from the crater S2. Most of the other stations clipped on the first explosion. Three other explosions were also very energetic with peak pressures exceeding 200 Pa. Infrasound signals were also used to describe the activity of individual vents in the days leading up to the major explosive event (Supplementary Material 1 Figure S1). This analysis was carried out using the reverse time migration (RTM) algorithm by Fee et al. [2021].

4 Results

The major explosive event on 13 May 2022 consisted of at least seven distinct explosions over two minutes as shown in Figure 3 and the thermal video of the permanent camera by LGS (Laboratorio di Geofisica Sperimentale*). Through the thermal video we can estimate the rough succession of explosive pulses, but it is not possible to establish exact locations for individual explosions. In the video, a second pulse originates farther from the northwest and appears to be inclined, suggesting a link to the vent in crater S1. Since all other vents are on a similar optical axis (from the point of view of the thermal camera), determining the source location relies on analysis of infrasound data [Fee et al. 2023]. During this event, an extensive amount of juvenile and reworked material was emitted.

*https://www.youtube.com/watch?v=7ixO_hZzGJ0; accessed 26/04/2024

Table 1: Survey information for the collection of the aerial imagery on 13 and 14 May 2022.

Data	Unit	Survey	
		13 May 2022	14 May 2022
Images		128	220
Flight altitude	m	92.2	99.8
Ground Sample Distance	cm pix^{-1}	2.4	2.5
Real Time Kinematic		Yes	No
Digital Elevation Model resolution	cm pix^{-1}	4.95	4.63
Orthomosaic resolution	cm pix^{-1}	2.48	2.31
Area	km^2	0.173	0.186
Reprojection error	pix	0.306	0.287
Camera location error	mm	5.75	54.76

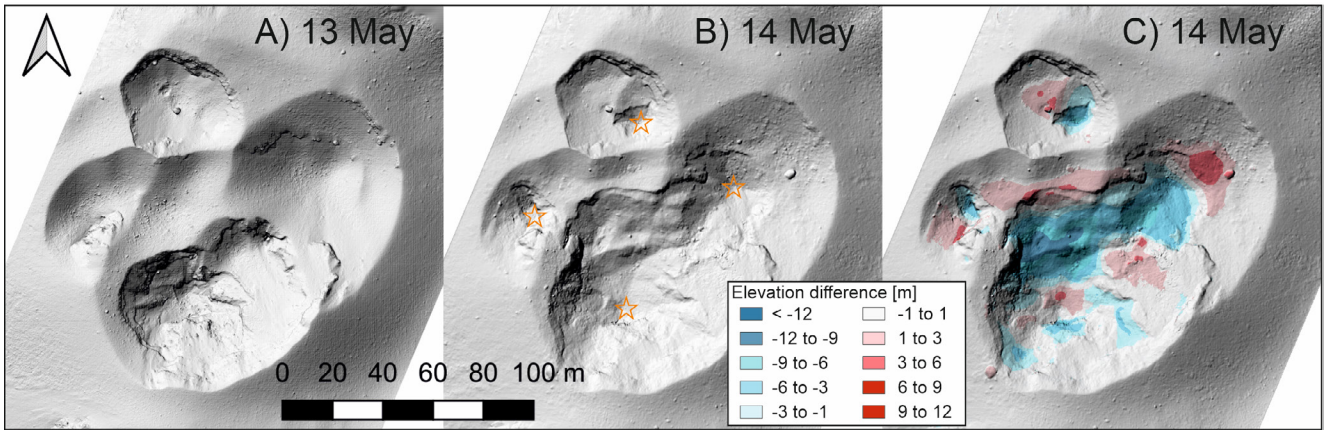

Figure 4: Time series highlighting the morphological changes of the crater terrace of Stromboli volcano, Italy. [A] and [B] show the DEM on 13 and 14 May 2022, respectively. Orange stars in B) show the locations of the post-explosion vents. The coloured overlay in [C] represents elevation difference between 13 and 14 May 2022. Blue colours represent elevation loss related to explosive excavation, and red hues signify elevation gain as a result of deposition of pyroclastic material during the 13 May 2022 major explosive event.

Our analysis of morphological changes reveals that four vents in crater CS were active (Figure 4). Whereas crater S2 showed activity in the days prior to the event, craters S1 and C were inactive. Within crater S2, two vents were active, causing the greatest changes, both erosional and depositional. Before the 13 May 2022 event, crater C contained a depression but without a visible vent location. As a result of the major explosive event, this area was partly excavated by one or more explosive pulses eroding the vent vertically by 9 m (Figure 5). In the northern part of crater C, up to 6 m of material were deposited. In the eastern part of crater S2, about 12 m of material were excavated by the explosion. Locally, between 1 and 6 m of material were deposited around its vent. Within crater S2, in the western portion up to 6 m were excavated at the vent location, while material was deposited around the vent with the thickest deposits forming at the base (northern side) of a rock outcrop (Figure 4C). Within crater S2, the western and eastern vents remain separated by a steep-sided ridge (Figure 5).

Within crater S1 up to 9 m of elevation was lost at the location of the new vent, while between 1 and 3 m were added in the position of the presumed former vent. The solidified lava plug within crater S1 (Figure 2) remained geometrically unchanged; the elevation changes indicated in Figure 4 are the result of the plug being pushed around two meters to the northwest by the explosion at the new vent location southeast of the plug. The plug remained intact but appears to be more inclined compared to its pre-event location. The topographic changes around the plug are attributed to the deposition of pyroclastic material in the crater S1.

We analysed the volumetric change induced by the major explosion on 13 May 2022 by calculating the volumes above and below the reference DEM (13 May 2022) for the new surface on 14 May 2022. In total, there was a volume difference of 12.7×10^3 m^3 through excavation and 5.5×10^3 m^3 of deposition by the explosive pulses within the craters of CS. The volumetric changes can also be estimated for each of the vent areas (S1, S2, C; Figure 1). Within crater S1 0.6×10^3 m^3 ($\pm 0.1 \times 10^3$ m^3) were deposited, and 0.6×10^3 m^3 ($\pm 0.1 \times 10^3$ m^3) excavated. In crater S2 the deposits have a volume of 3.0×10^3 m^3 ($\pm 0.2 \times 10^3$ m^3) and 9.2×10^3 m^3 ($\pm 0.7 \times 10^3$ m^3) were affected by excavation, respectively. In crater C, 1.8×10^3 m^3 ($\pm 0.2 \times 10^3$ m^3) were deposited and 3.0×10^3 m^3 ($\pm 0.3 \times 10^3$ m^3) excavated.

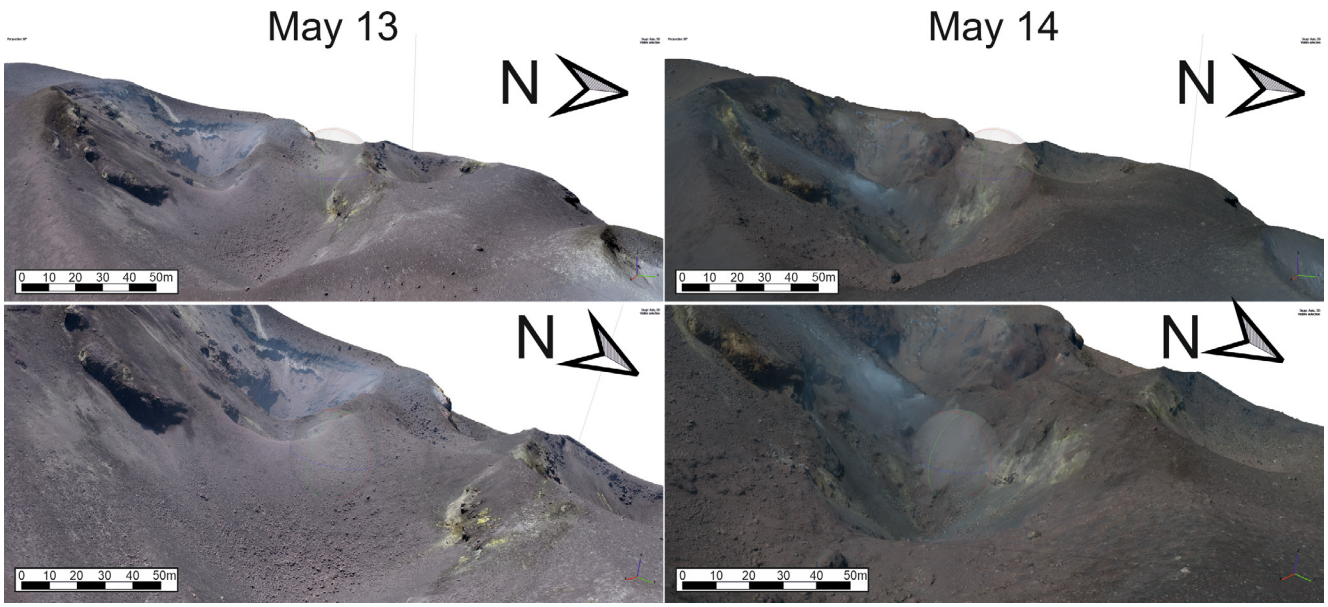

Figure 5: Views of the C and S2 craters in the 3D models created with `Agisoft Metashape` as visible on 13 and 14 May 2022, respectively. Areas of excavation and deposition can be identified. Before the explosive event, crater C contained a depression but without a visible vent location. Afterwards, this area was partly excavated by one or more explosive pulses eroding the vent vertically. In S2, excavation was dominating in the western portion. The areas of the western and eastern vents remain separated by a steep-sided ridge.

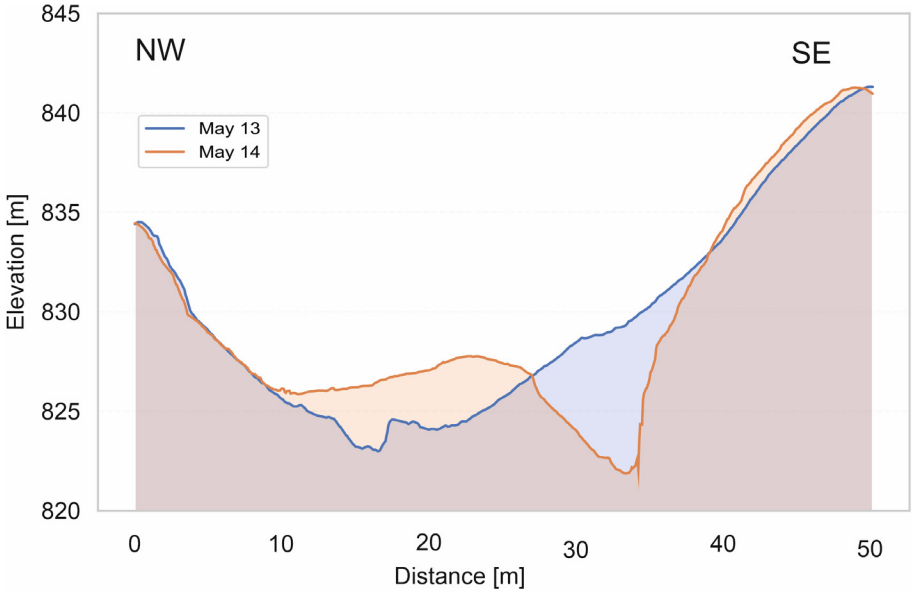

Figure 6: Section through S1 vent from NW to SE showing the surface changes induced by the 13 May 2022 major explosive event at Stromboli volcano, Italy. The blue line represents the surface two hours prior the event where the depression marks the location of the previous vent. The orange line represents the surface 19 hours after the event (14 May 2022), showing a shift in vent location of ~20 m towards the SE. The vent active during the major explosion shows an asymmetric geometry with a shallower angle towards the NW and as a result a preferential distribution of deposits towards the NW as well. A link between asymmetrical vent geometry and the related distribution of ballistics has been demonstrated experimentally [Schmid et al. 2022].

A profile through the S1 crater (Figure 6; see Figure 1 for the location of the profile) shows the morphology on 13 and 14 May and the related migration of the vent location (lowest point within the crater) of around 20 m to the SE. This profile also reveals the strong asymmetry of the new crater, which is responsible for the predominant dispersal of the ejected material to the northwest, locally causing ~3 m of deposition within the crater of S1 (Figure 4 and Figure 6). Supplementary Material 1 Figure S4 shows two cross-sections through the crater S2, one along a northeast-to-southwest profile (Figure 1 and Supplementary Material 1 Figure S4A) and another along a north-to-south profile (Figure 1 and Supplementary Material

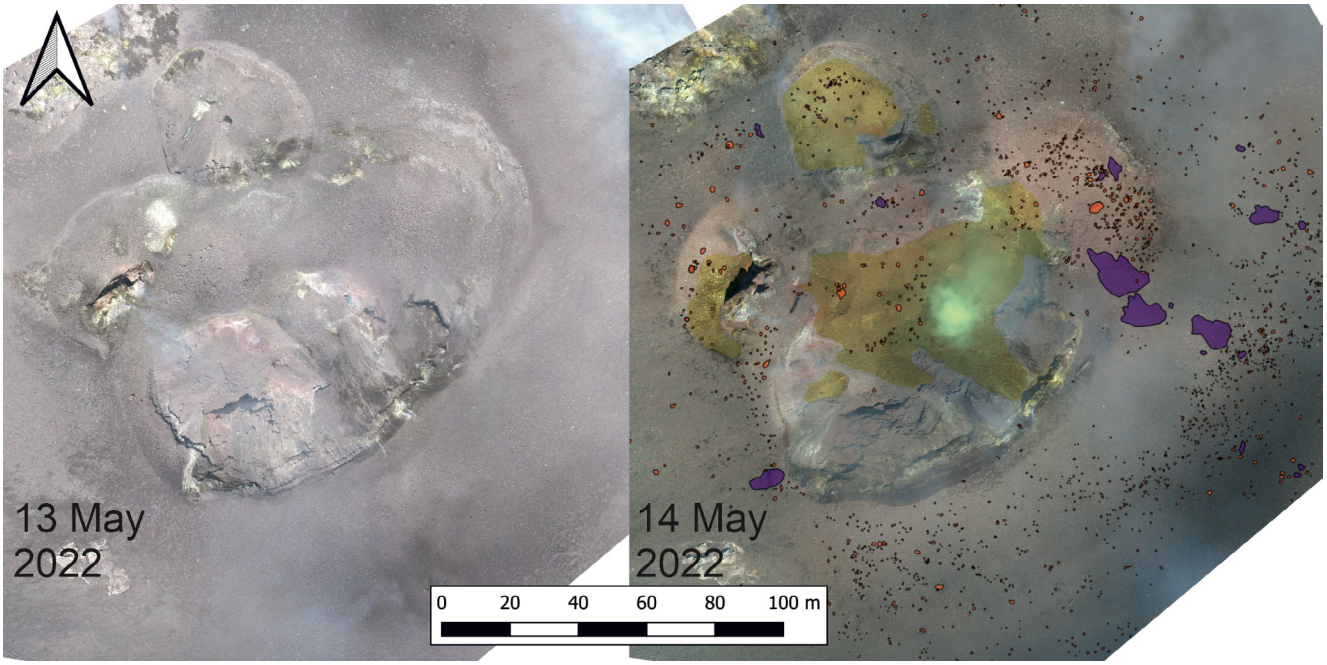

Figure 7: Comparison of orthomosaics on 13 and 14 May 2022. The orthomosaic of 14 May 2022 is overlain with a classification of pyroclastic deposits. The depressions within the crater terrace are covered entirely with pyroclastic deposits of variable sizes marked as talus (yellow areas). Distinct orange symbols classify lithic blocks larger than approximately 0.2 m. Purple symbols mark areas that are covered by spatter bombs.

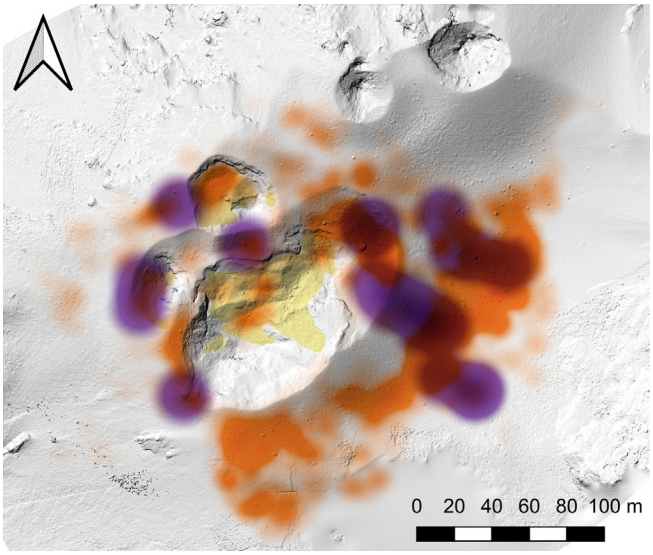

Figure 8: Heatmap of distribution of bombs larger than 0.2 m in the CS crater area. Yellow areas show talus where pyroclastic material accumulated. Orange colour hues signify the density distribution of blocks; purple shows the density distribution of spatter bombs. Map was created based on the QGIS kernel density distribution of the centroids of bombs mapped in Figure 7.

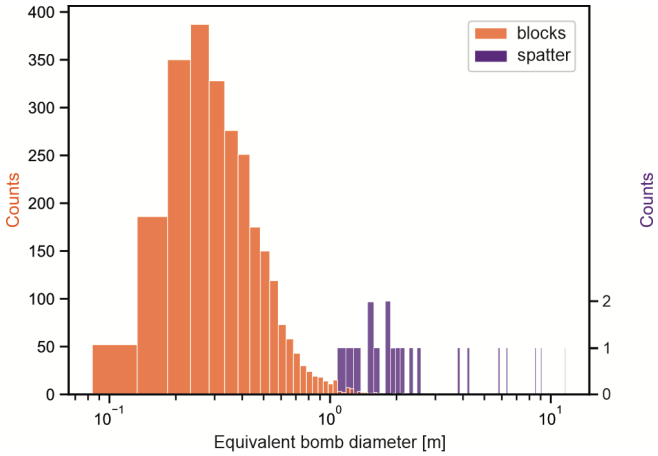

Figure 9: Size distribution of individual blocks and spatter bombs. Blocks are more numerous and in general smaller in size (average ~ 0.4 m); spatter bombs are sparse and significantly larger (average ~ 3.6 m).

1 Figure S4B). These profiles show the quality of DEM alignment and the (elevation) changes within the crater due to explosive excavation and deposition. The hump on top of the southwest rim of crater S2 (Supplementary Material 1 Figure S4A) represents a bomb that landed on the rim of the crater. Figures S4A, S4B (Supplementary Material 1) show slumping of material deposited during the major explosive event along the north side of crater S2.

The orthomosaics also allow tracking and classification of bombs with a diameter of roughly > 0.2 m (Figure 7). Although the areas affected by bombs extends beyond the area of interest depicted in Figure 7, it is still possible to qualitatively assess the distribution and the frequency distribution of blocks as well as spatter bombs. Depressions within the crater terrace were filled with debris and pyroclast deposits (talus, Fig-

ure 7). In total we measured 2657 bombs in the orthomosaic, 2637 were visually (by shape and surface) identified as angular blocks and 20 as spatter bombs (where the overall shape indicates ductile deformation after impact). Together they cover an area of 950 m^2, divided into 515 m^2 and 440 m^2 for blocks and spatter bombs, respectively. The bimodal distribution of bomb sizes, with a large number of small (< 0.5 m) blocks and only a few spatter bombs, yet with a larger average size (1–3 m) is shown in Figure 8. Furthermore, we approximated the volumes of blocks and spatter bombs in the area of interest (Figure 7) to be 370 m^3 and 90 m^3, respectively, by assuming a spherical shape for blocks and a thickness of 0.2 m for spatter bombs. The ratio between juvenile and lithic material for smaller clast sizes might be different. We interpret that most of the ejected blocks represent dense lithics that were produced by erosion of wall rock or the destruction of plugged conduits. Figure 9 shows a heatmap visualisation of the ballistic hazards around crater CS. Red and green hues show the density of block and spatter bomb impacts, respectively. It is noteworthy that bombs and pyroclasts were deposited well beyond the area shown in the figures presented here.

The high resolution of the aerial images also allowed a quantification of the size and diameter of the solidified lava plug that was protruding within crater S1 (Figure 2). The plug itself appears to be dense with several cracks. Its diameter is approximately 2.4 × 1.8 m with a height of 3.2 m above the crater floor (before the major explosive event). Here, the plug is located in the direct vicinity (within 5 m) of the pre-explosion location of the vent (Figure 2). As a result of the deposition of pyroclasts during the major event, the plug's height above the surrounding debris surface was reduced to around 1.0 m. This feature gives an insight in the geometry of the shallow plumbing system as it represents the minimum diameter of the subsurface (uppermost tens of meters) conduit section. The occurrence of this plug, as evidence for an older vent location, and the shift in vent location through the major explosion within crater S1 highlights the dynamic nature of the shallow plumbing system at Stromboli.

5 Discussion and Conclusions

Timely capture of imagery before and soon after the 13 May 2022 explosive event allowed us to acquire a dataset with high spatial and temporal resolution highlighting the morphological changes induced by a major explosion at Stromboli volcano with little contamination from background activity. The modified morphology demonstrates that four vents from crater CS were involved in at least seven explosions (Figure 3).

Here we quantified the volume differences by excavation and deposition within CS to be 12.7 × 10^3 m^3 and 5.5 × 10^3 m^3, respectively, and for each crater individually. Locally, up to ~12 m of elevation was lost while a maximum of ~6 m was gained. This dataset also highlights the ephemeral nature of the shallow plumbing system at Stromboli volcano with frequent changes of vent locations, especially evident in crater S1. Within this crater (42 × 49 m), we observe evidence for three different vent locations through the solidified remnant of a conduit (plug) and the shifting of vent positions relative to the plug before and after the major explosion.

By using high-resolution orthomosaics, we were able to determine the ratio of block and spatter bombs remotely. While this process is certainly less accurate than mapping deposits directly, it is the only possible option for gathering information about the type of explosive products in areas that cannot be accessed due to the inherent danger close to volcanic vents. In case of the major explosive event on 13 May 2022 the high number of blocks suggests a strong interaction with wall rock and/or fragmentation of solidified plugs in the shallow subsurface plumbing system. In contrast, characterised the bombs emplaced by the 21 January 2010 major explosion to be dominated by "fresh juvenile scoria with minor lithics of old scoria". This suggests that there might be different processes driving distinct major explosions at Stromboli. Repeated analyses of the ratios between different types of ballistics in future eruptions may provide insights into the shallow conduit dynamics and their variability that are controlling such explosive events. Furthermore, the distribution of bombs and pyroclastic deposits can be linked to the asymmetric geometry of the active crater S1 illustrating the strong effect of geometry on the dispersal of pyroclasts and related hazards [Schmid et al. 2022].

A combination of volumetric changes induced by individual explosive pulses derived by UAS surveys in combination with the related geophysical signals can aid in constraining the energy budget of volcanic explosions and refine mass flow estimates based on geophysical observations [Fee et al. 2017; Vossen et al. 2022]. Contemporary topographic models are also important during analyses of other datasets that benefit from geometrical constraints such as models of shallow and subaerial eruption processes and geophysical source location models.

Author Contributions

MS, UK, DF and MR conceptualized the study. MS, UK, VC, DF, JEG, AMI, CC, CEJV, RMB, MR and GL participated actively in the multiparametric field campaign (instrument transport and installation, maintenance and data download). MS conducted the UAS flights and processed the data. MS, UK, TR, RC, discussed morphological development of Stromboli volcano. DF, JEG and VC provided information about acoustic and infrasound observations. MS, UK and DF discussed morphological and infrasound data. MR and GL helped with the logistics of the campaign. D.B.D provided funding and reviewed the manuscript. All authors discussed the data and agreed on the manuscript.

Acknowledgements

We acknowledge the support of the European Research Council Advanced Grant ERC-2018-ADG No. 834225 "EAVESDROP" (Schmid, Dingwell), project CI306/2-1 from the Deutsche Forschungsgemeinschaft (German Science Foundation) (Cigala, Kueppers, and Schmid), and ERC-Con nr. 864052 "VOLTA" (Cimarelli and Vossen), and NSF Grants EAR-1901614 (Fee and Gestrich), EAR-1952392 (Iezzi) and the INGV Departmental Strategic Project UNO (Ricci and Civico). Any use of trade, firm, or product names is for descriptive purposes only and does not imply endorsement by the U.S. Government.

Data Availability

The processed DEMs and orthomosaics as well as the aerial imagery used for this study can be made available through contacting the corresponding author. Infrasound data are available on IRIS with temporary network code "ZV" (Fee et al. [2022], https://www.fdsn.org/networks/detail/ZV_2022/.

Copyright notice

References

Andronico, D., E. Del Bello, C. D'Oriano, P. Landi, F. Pardini, P. Scarlato, M. de'Michieli Vitturi, J. Taddeucci, A. Cristaldi, F. Ciancitto, F. Pennacchia, T. Ricci, and F. Valentini (2021). "Uncovering the eruptive patterns of the 2019 double paroxysm eruption crisis of Stromboli volcano". *Nature Communications* 12(1). DOI: 10.1038/s41467-021-24420-1.

Barberi, F. (1993). "Volcanic hazard assessment at Stromboli based on review of historical data." *Acta Vulcanologica* 3, pages 173–187.

Bertagnini, A., A. Di Roberto, and M. Pompilio (2011). "Paroxysmal activity at Stromboli: lessons from the past". *Bulletin of Volcanology* 73(9), pages 1229–1243. DOI: 10.1007/s00445-011-0470-3.

Bevilacqua, A., L. Nannipieri, M. Favalli, and A. Fornaciai (2024). "UAS-based mapping of the July 3, 2019, ballistics density distribution on the W flank of Stromboli with uncertainty quantification". *Bulletin of Volcanology* 86(5). DOI: 10.1007/s00445-024-01741-9.

Bevilacqua, A., A. Bertagnini, M. Pompilio, P. Landi, P. Del Carlo, A. Di Roberto, W. Aspinall, and A. Neri (2020). "Major explosions and paroxysms at Stromboli (Italy): a new historical catalog and temporal models of occurrence with uncertainty quantification". *Scientific Reports* 10(1). DOI: 10.1038/s41598-020-74301-8.

Bisson, M., C. Spinetti, R. Gianardi, K. Strehlow, E. De Beni, and P. Landi (2023). "High-resolution mapping and dispersion analyses of volcanic ballistics emitted during the 3rd July 2019 paroxysm at Stromboli". *Scientific Reports* 13(1). DOI: 10.1038/s41598-023-39600-w.

Calvari, S., R. BÃ¼ttner, A. Cristaldi, P. Dellino, F. Giudicepietro, M. Orazi, R. Peluso, L. Spampinato, B. Zimanowski, and E. Boschi (2012). "The 7 September 2008 Vulcanian explosion at Stromboli volcano: Multiparametric characterization of the event and quantification of the ejecta". *Journal of Geophysical Research: Solid Earth* 117(B5). DOI: 10.1029/2011jb009048.

Calvari, S. and G. Nunnari (2023). "Statistical Insights on the Eruptive Activity at Stromboli Volcano (Italy) Recorded from 1879 to 2023". *Remote Sensing* 15(19), page 4822. DOI: 10.3390/rs15194822.

Civico, R., T. Ricci, A. Cecili, and P. Scarlato (2024). "High-resolution topography reveals morphological changes of Stromboli volcano following the July 2024 eruption". *Scientific Data* 11(1). DOI: 10.1038/s41597-024-04098-y.

Civico, R., T. Ricci, P. Scarlato, D. Andronico, M. Cantarero, B. B. Carr, E. De Beni, E. Del Bello, J. B. Johnson, U. Kueppers, L. Pizzimenti, M. Schmid, K. Strehlow, and J. Taddeucci (2021). "Unoccupied Aircraft Systems (UASs) Reveal the Morphological Changes at Stromboli Volcano (Italy) before, between, and after the 3 July and 28 August 2019 Paroxysmal Eruptions". *Remote Sensing* 13(15), page 2870. DOI: 10.3390/rs13152870.

Darmawan, H., T. R. Walter, K. S. Brotopuspito, Subandriyo, and I. G. M. A. Nandaka (2018). "Morphological and structural changes at the Merapi lava dome monitored in 2012–15 using unmanned aerial vehicles (UAVs)". *Journal of Volcanology and Geothermal Research* 349, pages 256–267. DOI: 10.1016/j.jvolgeores.2017.11.006.

De Beni, E., M. Cantarero, and A. Messina (2019). "UAVs for volcano monitoring: A new approach applied on an active lava flow on Mt. Etna (Italy), during the 27 February–02 March 2017 eruption". *Journal of Volcanology and Geothermal Research* 369, pages 250–262. DOI: 10.1016/j.jvolgeores.2018.12.001.

Dietterich, H. R., A. K. Diefenbach, S. A. Soule, M. H. Zoeller, M. P. Patrick, J. J. Major, and P. R. Lundgren (2021). "Lava effusion rate evolution and erupted volume during the 2018 Kilauea lower East Rift Zone eruption". *Bulletin of Volcanology* 83(4). DOI: 10.1007/s00445-021-01443-6.

Eltner, A., A. Kaiser, C. Castillo, G. Rock, F. Neugirg, and A. Abellán (2016). "Image-based surface reconstruction in geomorphometry – merits, limits and developments". *Earth Surface Dynamics* 4(2), pages 359–389. DOI: 10.5194/esurf-4-359-2016.

Fee, D., Alexandra Iezzi, and Julia Gestrich (2022). "Stromboli volcano Temporary Deployment, May 2022". *International Federation of Digital Seismograph Networks*. DOI: 10.7914/K4H6-VZ20. [Dataset].

Fee, D., V. Cigala, C. Cimarelli, J. E. Gestrich, A. M. Iezzi, U. Kueppers, G. Lacanna, M. Ripepe, M. Schmid, and C. E. J. Vossen (2023). "Dense infrasound and multiparameter observations of the May 13, 2022 major explosion of Stromboli Volcano, Italy". *IAVCEI 2023 Scientific Assembly Book of Abstracts*. 447. Rotorua, New Zealand: International Association of Volcanology and Chemistry of the Earth's Interior, page 316.

Fee, D., P. Izbekov, K. Kim, A. Yokoo, T. Lopez, F. Prata, R. Kazahaya, H. Nakamichi, and M. Iguchi (2017). "Eruption mass estimation using infrasound waveform inversion and ash and gas measurements: Evaluation at Sakurajima Volcano, Japan". *Earth and Planetary Science Letters* 480, pages 42–52. DOI: 10.1016/j.epsl.2017.09.043.

Fee, D., L. Toney, K. Kim, R. W. Sanderson, A. M. Iezzi, R. S. Matoza, S. De Angelis, A. D. Jolly, J. J. Lyons, and M. M. Haney (2021). "Local Explosion Detection and Infrasound Localization by Reverse Time Migration Using 3-D Finite-Difference Wave Propagation". *Frontiers in Earth Science* 9. DOI: 10.3389/feart.2021.620813.

Galle, B., S. Arellano, N. Bobrowski, V. Conde, T. P. Fischer, G. Gerdes, A. Gutmann, T. Hoffmann, I. Itikarai, T. Krejci, E. J. Liu, K. Mulina, S. Nowicki, T. Richardson, J. Rüdiger, K. Wood, and J. Xu (2021). "A multi-purpose, multi-rotor drone system for long-range and high-altitude volcanic gas plume measurements". *Atmospheric Measurement Techniques* 14(6), pages 4255–4277. DOI: 10.5194/amt-14-4255-2021.

Gestrich, J. E., D. Fee, A. M. Iezzi, U. Kueppers, M. Schmid, C. E. J. Vossen, C. Cimarelli, M. Ripepe, G. Lacanna, and R. M. Buzard (2023). "Acoustic Resonances and Jet Noise of Stromboli Volcano". *AGU Fall Meeting Abstracts*. Volume 2023, V11D-0102, pages V11D–0102.

Giordano, G. and G. De Astis (2021). "The summer 2019 basaltic Vulcanian eruptions (paroxysms) of Stromboli". *Bulletin of Volcanology* 83(1). DOI: 10.1007/s00445-020-01423-2.

Giudicepietro, F., C. LÃ³pez, G. Macedonio, S. Alparone, F. Bianco, S. Calvari, W. De Cesare, D. Delle Donne, B. Di Lieto, A. M. Esposito, M. Orazi, R. Peluso, E. Privitera, P. Romano, G. Scarpato, and A. Tramelli (2020). "Geophysical precursors of the July-August 2019 paroxysmal eruptive phase and their implications for Stromboli volcano (Italy) monitoring". *Scientific Reports* 10(1). DOI: 10.1038/s41598-020-67220-1.

Iezzi, A. M., R. M. Buzard, D. Fee, R. S. Matoza, J. E. Gestrich, A. D. Jolly, M. Schmid, V. Cigala, U. Kueppers, C. E. J. Vossen, C. Cimarelli, G. Lacanna, and M. Ripepe (2023). "UAS-Based Observations of Infrasound Directionality at Stromboli Volcano, Italy". *Geophysical Research Letters* 50(8). DOI: 10.1029/2023gl102905.

James, M. R., B. Carr, F. D'Arcy, A. Diefenbach, H. Dietterich, A. Fornaciai, E. Lev, E. Liu, D. Pieri, M. Rodgers, B. Smets, A. Terada, F. Von Aulock, T. Walter, K. Wood, and E. Zorn (2020a). "Volcanological applications of unoccupied aircraft systems (UAS): Developments, strategies, and future challenges". *Volcanica* 3(1), pages 67–114. DOI: 10.30909/vol.03.01.67114.

James, M. R., G. Antoniazza, S. Robson, and S. N. Lane (2020b). "Mitigating systematic error in topographic models for geomorphic change detection: accuracy, precision and considerations beyond off-nadir imagery". *Earth Surface Processes and Landforms* 45(10), pages 2251–2271. DOI: 10.1002/esp.4878.

James, M. R., J. H. Chandler, A. Eltner, C. Fraser, P. E. Miller, J. P. Mills, T. Noble, S. Robson, and S. N. Lane (2019). "Guidelines on the use of structure-from-motion photogrammetry in geomorphic research". *Earth Surface Processes and Landforms* 44(10), pages 2081–2084. DOI: 10.1002/esp.4637.

Lev, E. (2022). "UAVs in Volcanology". *UAVs for the Environmental Sciences: Methods and Applications*. Edited by A. Eltner, D. Hoffmeister, A. Kaiser, P. Karrasch, L. Klingbeil, C. Stöcker, and A. Rovere. Darmstadt: wbg (Wissenschaftliche Buchgesellschaft)) Aademic. Chapter 4.6, pages 379–392. ISBN: 978-3-534-40588-6.

Liu, E. J., K. Wood, E. Mason, M. Edmonds, A. Aiuppa, G. Giudice, M. Bitetto, V. Francofonte, S. Burrow, T. Richardson, M. Watson, T. D. Pering, T. C. Wilkes, A. J. S. McGonigle, G. Velasquez, C. Melgarejo, and C. Bucarey (2019). "Dynamics of Outgassing and Plume Transport Revealed by Proximal Unmanned Aerial System (UAS) Measurements at Volcán Villarrica, Chile". *Geochemistry, Geophysics, Geosystems* 20(2), pages 730–750. DOI: 10.1029/2018gc007692.

MacLeod, J., K. Wood, T. Rendall, M. Watson, C. Allen, M. Reader, J. Lucas, and T. Richardson (2023). "Design of a collector for sampling volcanic ash using unmanned aerial systems". *Journal of Aerosol Science* 169, page 106119. DOI: 10.1016/j.jaerosci.2022.106119.

Nadeau, P., A. Diefenbach, S. Hurwitz, and D. Swanson (2020). "From Lava to Water: A New Era at Kīlauea". *Eos* 101. DOI: 10.1029/2020eo149557.

Over, J.-S. R., A. C. Ritchie, C. J. Kranenburg, J. A. Brown, D. D. Buscombe, T. Noble, C. R. Sherwood, J. A. Warrick, and P. A. Wernette (2021). *Processing coastal imagery with Agisoft Metashape Professional Edition, version 1.6—Structure from motion workflow documentation*. DOI: 10.3133/ofr20211039.

Ripepe, M., G. Lacanna, M. Pistolesi, M. C. Silengo, A. Aiuppa, M. Laiolo, F. Massimetti, L. Innocenti, M. Della Schiava, M. Bitetto, F. P. La Monica, T. Nishimura, M. Rosi, D. Mangione, A. Ricciardi, R. Genco, D. Coppola, E. Marchetti, and D. Delle Donne (2021). "Ground deformation reveals the scale-invariant conduit dynamics driving explosive basaltic eruptions". *Nature Communications* 12(1). DOI: 10.1038/s41467-021-21722-2.

Ripepe, M., D. D. Donne, A. Harris, E. Marchetti, and G. Ulivieri (2008). "Dynamics of Strombolian Activity". *The Stromboli Volcano: An Integrated Study of the 2002–2003 Eruption*. Edited by S. Calvar, S. Inguaggiato, G. Puglisi, M. Ripepe, and M. Rosi. American Geophysical Union, pages 39–48. DOI: 10.1029/182gm05.

Rosi, M., A. Bertagnini, and P. Landi (2000). "Onset of the persistent activity at Stromboli Volcano (Italy)". *Bulletin of Volcanology* 62(4–5), pages 294–300. DOI: 10.1007/s004450000098.

Rosi, M., M. Pistolesi, A. Bertagnini, P. Landi, M. Pompilio, and A. Di Roberto (2013). "Stromboli volcano, Aeolian Islands (Italy): present eruptive activity and hazards". *The Aeolian Islands Volcanoes*. Edited by F. Lucchi, A. Peccerillo, J. Keller, C. A. Tranne, and P. L. Rossi. Volume 37. 1. Geological Society of London. Chapter 14, pages 473–490. DOI: 10.1144/m37.14.

Schmid, M., U. Kueppers, V. Cigala, and D. B. Dingwell (2022). "Complex geometry of volcanic vents and asymmetric particle ejection: experimental insights". *Bulletin of Volcanology* 84(8). DOI: 10.1007/s00445-022-01580-6.

Schmid, M., U. Kueppers, R. Civico, T. Ricci, J. Taddeucci, and D. B. Dingwell (2021). "Characterising vent and crater shape changes at Stromboli: implications for risk areas". *Volcanica* 4(1), pages 87–105. DOI: 10.30909/vol.04.01.87105.

Schmid, M., U. Kueppers, J. Huber, and D. B. Dingwell (2023). "Drone deployed sensors: a tool for multiparametric near-vent measurements of volcanic explosions". *Volcanica* 6(1), pages 95–106. DOI: 10.30909/vol.06.01.95106.

Turner, N., B. Houghton, J. Taddeucci, J. von der Lieth, U. Kueppers, D. Gaudin, T. Ricci, K. Kim, and P. Scalato (2017). "Drone Peers into Open Volcanic Vents". *Eos*. DOI: 10.1029/2017eo082751.

Visalli, R., M. Giuffrida, and M. Viccaro (2023). "Unraveling Textural and Chemical Features in Volcanic Rocks Through Advanced Image Processing: A Case Study From the 2019 Paroxysmal Eruptions of Stromboli". *Geochemistry, Geophysics, Geosystems* 24(3). DOI: 10.1029/2022gc010774.

Vossen, C. E. J., C. Cimarelli, A. J. Bennett, M. Schmid, U. Kueppers, T. Ricci, and J. Taddeucci (2022). "The electrical signature of mafic explosive eruptions at Stromboli volcano, Italy". *Scientific Reports* 12(1). DOI: 10.1038/s41598-022-12906-x.

Zorn, E. U., T. R. Walter, J. B. Johnson, and R. Mania (2020). "UAS-based tracking of the Santiaguito Lava Dome, Guatemala". *Scientific Reports* 10(1). DOI: 10.1038/s41598-020-65386-2.